

## 3D Network Conductive Polymer/Pt Composites as Electrocatalyst for Methanol Oxidation

Maodan Xu<sup>1</sup>, Yongquan Qing<sup>2</sup>, Yanbin Yin<sup>1</sup>, Shiyun Ai<sup>1</sup>, Junling Duan<sup>1</sup>, Houshen Li<sup>1,\*</sup> and Yijing Li<sup>1,\*</sup>

<sup>1</sup> College of Chemistry and Material Science, Shandong Agricultural University, Taian, Shandong, 271018, PR China.

<sup>2</sup> Key Laboratory for Anisotropy and Texture of Materials, Ministry of Education, Northeastern University, Shenyang 110819, China.

\*E-mail: [hslis@sdau.edu.cn](mailto:hslis@sdau.edu.cn), [yjli@sdau.edu.cn](mailto:yjli@sdau.edu.cn)

Received: 3 September 2019 / Accepted: 29 October 2019 / Published: 30 November 2019

---

Methanol oxidation is a fatal reaction for developing methanol-based fuel cell, which is an potential choice for solving energy crisis. Here, we developed a simple and efficient strategy for synthesis of three-dimensional (3D) network polyaniline (PANI) gel which was used as conductive matrix for methanol oxidation. Then, we systematically compared the electrochemical activity of differently shaped Pt nanomaterials. Due to the combination of the specific structure of Pt nanomaterial, conducting properties and large surface of 3D network PANI, 3D PANI/Pt NCs catalyst shows excellent electrocatalysis performance. In comparison with commercial Pt black, hyperbranched Pt NCs, and other structure PANI/Pt NCs, the 3D network PANI/Pt NCs have superior catalytic activity and stability towards methanol oxidation. The catalytic activity of 3D network PANI/Pt NCs was 2.92 times higher than that of the commercial Pt black. Besides, the original 3D network PANI also shows well Cr(VI) removal properties due to its large surface area and abundant active sites. Meanwhile, the 3D network PANI with simple fabrication process and excellent performance may have great potential in electrochemical applications and biosensors.

---

**Keywords:** energy crisis, fuel cell, Pt, conductive polymer, heavy metal removal.

### 1. INTRODUCTION

Energy crisis and environmental problems are two fatal challenges human face today [1,2]. So, it is meaningful to find high-efficient and sustainable methods to use natural resources. Based on this, direct fuel cells (DFCs), such as direct alcohol fuel cells (DAFCs) or direct methanol fuel cells (DMFCs), have received great attentions as powerful and clean electrochemical energy converters for electric vehicles and portable electronic devices due to their high energy conversion efficiency, ambient

operating conditions, and environmental friendliness [3,4]. However, the performance of DFCs is limited by the insufficient electrocatalytic activity and poor durability of catalyst [5]. At present, Pt-based electrocatalysts are still regarded as the most effective anode electrocatalysts for DFCs due to their high electrocatalytic activities [6-8], but the high price of Pt metal make it hard to use Pt as catalysts in wide application. Therefore, recent studies always focused on the utilization of Pt in higher efficient way [9-11]. Recently, compositions, sizes, and morphologies of Pt nanomaterials are designed for tailoring the catalytic performance of electrocatalysts [12-15]. Although high-quality Pt-based catalysts with different morphologies, including nanodendrites [16,17], nanotubes [18], nanopolyhedra [19,20], nanocages [21] or nanowires [22] have been synthesized, the ligand surface coating during the synthesis process has always limited the range of the technical applicability of as-prepared Pt-based materials in electrocatalysis, especially organic ligand.

To date, the commercial catalysts for methanol oxidation are highly dispersed 2-5 nm Pt nanocrystals (NCs) supported on carbon matrix [23,24]. However, because of the corrosion of carbon support, Pt NCs always demonstrate poor durability and Pt aggregation. Thus, developing both high mass activity and good durability of Pt-based catalysts remains a challenge.

Conducting polymers such as polyaniline (PANI) have received attentions in fuel cell applications owing to their unique  $\pi$ -conjugated structures, good environmental stability, high electrical and proton conductivity in acidic environments [25]. In recent years, PANI has been used as supporting materials for constructing Pt-based catalyst owing to their notable electrical conductivity [26-28]. Recently, Jin synthesized 300-600 nm spherical Pt NCs on the surface of 2D PANI film consist of PANI nanofiber and show good catalytic activity to methanol oxidation [29]. Moreover, 3D conducting polymer such as PANI can provide interface between conducting matrix and the solution [30]. Yu group has done much work in synthesis of 3D PANI hydrogel and application in biosensor electrode materials to detect all metabolites simultaneously with high sensitivity and short response time [31-33]. But there are two key problems need to be solved: (1) the conventional chemical oxidative polymerization of aniline to synthesize PANI gel is carried out at cool temperature. The temperature is a key factor to form network gel. We intend to quickly synthesize the 3D network PANI gel at room temperature. (2) As far as possible to maximize the utilization ratio of platinum nanocrystals using 3D network PANI gel as supporting materials.

Herein, we firstly developed a simple and efficient strategy to synthesize 3D network PANI gel using CTAC or DTAC as template, APS as initiator, and formic acid as dopant. The 3D network PANI also shows well Cr(VI) removal properties due to its large surface area and abundant active sites. Then, small Pt NCs are grown directly onto the surface of 3D network PANI. Due to the conducting properties and large surface area of 3D network PANI, 3D network PANI/Pt NCs shows excellent electrocatalysis performance. Compared with commercial Pt black, hyperbranched Pt NCs, 1D PANI nanofiber/Pt NCs, and PANI hydrogel/Pt NCs, the obtained 3D network PANI/Pt NCs have superior catalytic activity and stability towards methanol oxidation. Meanwhile, the 3D network PANI with simple fabrication process and excellent performance may have great potential in electrochemical applications and biosensors.

## 2. EXPERIMENTAL SECTION

### 2.1 Chemicals and materials

Potassium tetrachloroplatinate (II) ( $K_2PtCl_4$ , 99%) and commercial Pt black (nominally 10% on carbon black) were purchased from Alfa Aesar (Tianjin, China). Aniline, ammonium persulfate (APS), cetyltrimethylammonium chloride (CTAC), dodecyltrimethylammonium chloride (DTAC), potassium dichromate ( $K_2Cr_2O_7$ ), and formic acid were purchased from Sinopharm Chemical Reagent Co. Ltd. Water used in all experiments was prepared in a three-stage Millipore Milli-Q plus 185 purification system and had a resistivity higher than 18.2 M $\Omega$  cm.

### 2.2 Synthesis of 3D network PANI gel

A fabrication process of 3D network PANI gel is given: 0.48 g of CTAC was dissolved in 2 mL of formic acid (used as the solvent and dopant) at room temperature. Next, 137  $\mu$ L of aniline monomer was added to the solution under stirring. After homogeneous mixing, 1 mL of ammonium persulfate (APS) solution (1.5 M) was added to the mixture solution under stirring. Then, the color of result mixture changed to dark green and formed to 3D network PANI gel under static condition for a few seconds at room temperature. Finally, after washing with water to remove the residual surfactant, the 3D Network CTAC-PANI was prepared with vacuum freeze drying for 12 hours. The synthesis protocol of 3D network DTAC-PANI gel is similar to the above method except that the mass of DTAC changed to 0.32 g.

### 2.3 Synthesis of 3D network PANI/Pt NCs

In a typical procedure, 3D network PANI with certain mass and 250  $\mu$ L of  $K_2PtCl_4$  solution (0.025 M) were added to 3.00 mL of water solution under stirring. Few minutes later, 750  $\mu$ L of formic acid was added into the mixed solution containing Pt precursor. Then, when the color of the reaction solutions gradually changed from green to dark, 3D network PANI/Pt NCs were obtained. The whole fabrication process was depicted in Scheme 1. The initial PANI contents was used for identify the prepared catalyst. The aniline monomer concentration is 0.56 mM, 2.81 mM, and 3.75 mM in 4 mL solution of synthesis of 3D network PANI/Pt NCs, respectively.

### 2.4 Characterization

Transmission electron microscopy (TEM) and high-resolution TEM (HRTEM) images were obtained with a JEOL JEM-2100F transmission electron microscope operating at an acceleration voltage of 200 kV. Elemental mapping images were acquired by energy dispersive X-ray spectroscopy (EDS) using a JEOL JEM-2100F electron microscope equipped with a STEM unit. The surface functional groups in samples were measured by Fourier transform infrared (FTIR) using a Thermo Scientific

Nicolet 380 spectrometer (USA). The absorption spectra were recorded by UV-Vis spectroscopy with a Cary 50 spectrophotometer using 10 mm path length quartz cuvettes.

### 2.5 Adsorption experiments

In the adsorption experiment, 10 mg of the adsorbents was mixed with 50 mL of Cr(VI) solution ( $C_0 = 50 \text{ mg L}^{-1}$ ) at different pH values (from 2 to 6) under 150 rpm shaking at room temperature. The concentrations of Cr(VI) were measured by 1,5-diphenylcarbazide colorimetric method, using a UV-Vis spectrophotometer at  $\lambda = 540 \text{ nm}$ . The Cr(VI) removal percentage ( $W\%$ ) is calculated using Eq. (1) :

$$W\% = \frac{C_0 - C_t}{C_0} \times 100 \quad (1)$$

where  $C_0$  (mg/L) is the initial Cr(VI) concentration, and  $C_t$  (mg/L) is the Cr(VI) concentration in solution at the contact time  $t$ . The removal capacity ( $Q_t$ , mg/g) is quantified by Eq. (2) :

$$Q_t = \frac{(C_0 - C_t)V}{m} \quad (2)$$

where  $V$  (mL) represents the volume of chromium solution, and  $m$  (mg) stands for the mass of the used adsorbent.

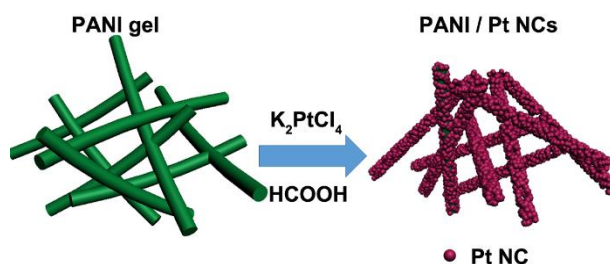
### 2.6 Electrochemical measurements

Cyclic voltammetry (CV) and chronoamperometric (CA) experiments were performed in a standard three-electrode cell in a CHI660E workstation at room temperature. Glassy carbon electrodes (GCE) modified by as-prepared 3D network PANI/Pt NCs were employed as the working electrode while an Ag/AgCl electrode and Pt wire were used as the reference electrode and auxiliary electrode, respectively. Before rinsed with pure water and dried at room temperature, the bare GCE was polished successively with 0.3 and 0.05 mm alumina slurries.

The preparation process of 3D network PANI/Pt NCs modified GCE: 6  $\mu\text{L}$  of PANI/Pt NCs solution was drop-coated on a freshly prepared bare GCE, followed by drying in air. 10  $\mu\text{L}$  of Nafion solution (0.2 wt% in ethanol) was cast on the surface of the modified GCE, followed by drying in air.

Cyclic voltammograms (CV) for determination of the electrochemically active surface area (ECSA) were recorded between -0.2 V and 1.2 V in  $\text{N}_2$ -saturated 0.5 M  $\text{H}_2\text{SO}_4$  solution with a scan rate of  $50 \text{ mV s}^{-1}$ . For methanol oxidation tests, CV measurements between 0 V and 1.0 V at a scan rate of  $20 \text{ mV s}^{-1}$  were recorded ( $\text{N}_2$ -saturated 0.5 M  $\text{H}_2\text{SO}_4$  and 1.0 M methanol solution). The ECSA was calculated by measuring the charge collected in the hydrogen adsorption/desorption region after double-layer correction and assuming a value of  $0.21 \text{ mC cm}^{-2}$  for the adsorption of a hydrogen monolayer [25]. Their mass current densities were normalized by the loaded Pt amounts of each catalyst.

### 3. RESULTS AND DISCUSSION



**Scheme 1.** Schematic illustration of the fabrication process of 3D network PANI/Pt NCs.

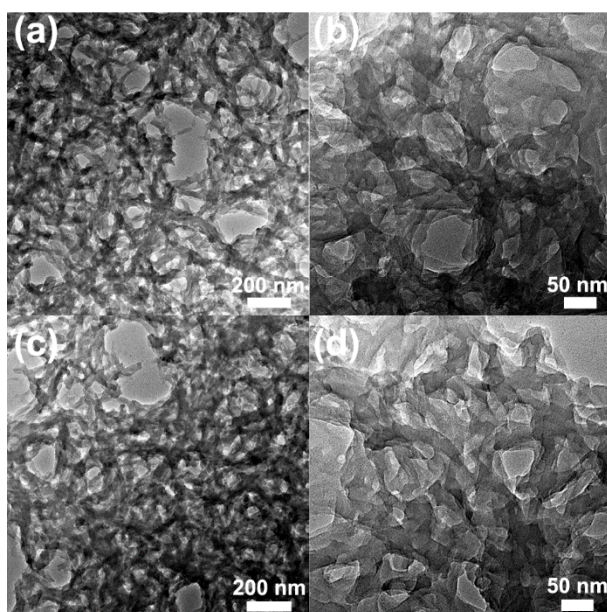


**Figure 1.** Different magnification TEM images of 3D network CTAC-PANI (a low and b high magnification) and DTAC-PANI (c low and d high magnification) gel.

*Synthesis of 3D network PANI gel.* The three-dimensional network PANI gel was synthesized by mixing solution of formic acid, CTAC (or DTAC), aniline monomer, and APS solution at room temperature. The mixed precursor solution's color changed to dark green, and the solution was gelled to form a gel within several seconds (Fig. S1). Fig. 1 show typical TEM images of the prepared PANI gel using CTAC (Fig. 1a and 1b) and DTAC (Fig. 1c and 1d) as template. The three-dimensional (3D) network microstructure were consisted of interconnected uniform PANI nanofibers with diameters of approximately 40 nm. We report a unique template approach for rapid synthesis of 3D network PANI at room temperature. The FTIR spectrum of 3D network PANI gel was also studied: spectrum of 3D network CTAC-PANI gel (Fig. S2a) shows that the characteristic peaks of PANI around  $1645\text{ cm}^{-1}$ ,  $1488\text{ cm}^{-1}$  (C=C stretching deformation of quinoid and benzenoid ring, respectively),  $1309\text{ cm}^{-1}$  (C–N stretching of secondary aromatic amine),  $1142\text{ cm}^{-1}$ , and  $796\text{ cm}^{-1}$  (out-of-plane deformation of C–H in the substituted benzene ring) [34]. The 3D network DTAC-PANI gel has the similar FTIR spectrum ( $1581$ ,  $1495$ ,  $1301$ ,  $1141$  and  $809\text{ cm}^{-1}$ , Fig. S2b). The slight shifts of the vibration bands of the 3D

network PANI gel may be caused by the chemical interaction and longer effective conjugation lengths [35].

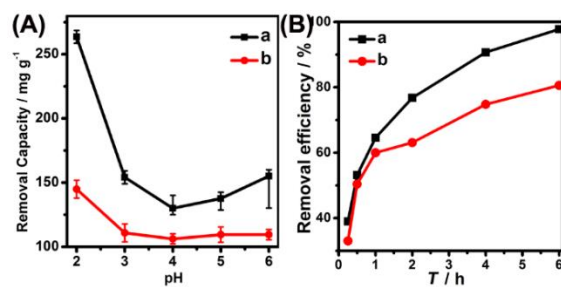


**Figure 2.** Effect of pH (A) and contact time (B) of CTAC-PANI (a, black curve) and DTAC-PANI (b, red curve) gel on removal of Cr(VI). The Cr(VI) concentration ( $C_0$ ) is  $50 \text{ mg L}^{-1}$  at room temperature.

The Cr(VI) adsorption experiment also been performed to examine the the Cr(VI) removal property of prepared 3D network PANI adsorbents. Because it can control the surface charge and the protonation degree of the adsorbent, pH is critical for Cr(VI) adsorption. As shown in Fig. 2A, the highest adsorption capacity ( $Q_t$ ) of 3D network CTAC-PANI and DTAC-PANI is  $263.5 \text{ mg g}^{-1}$  and  $145 \text{ mg g}^{-1}$  at the initial pH = 2, respectively. The Cr(VI) removal capacity gradually reaches equilibrium after pH = 4. The adsorption capacity of 3D network CTAC-PANI is higher than the adsorption capacity of other PANI-based adsorbents [36]. Entire 3D network PANI are protonated in low pH solution, enhancing electrostatic attraction between adsorbents and  $\text{HCrO}_4^-$ , and then anion adsorption occurs. The effect of contact time on removal of Cr(VI) between 3D network CTAC-PANI and DTAC-PANI also been investigated and shown in Fig. 2B. It can be easily found that The Cr(VI) adsorption capacity increases sharply at the initial period, then the slope of the curve decreases, and gradually reaches equilibrium. Results shown that the Cr(VI) removal capacity and efficiency of 3D network CTAC-PANI is more effectively than that of DTAC-PANI. The Cr(VI) removal properties of adsorbents can be attributed to the surface area, pore volume and size, as well as active sites for Cr(VI) adsorption. Thus, the microstructure of 3D network CTAC-PANI may have larger surface area or more active sites, which play important roles in the adsorption process.

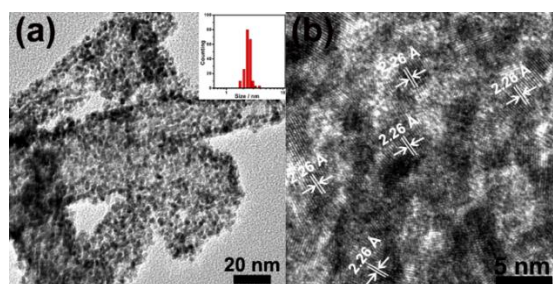


**Figure 3.** TEM (a) and HRTEM (b) images of 3D network PANI/Pt NCs. The insert is the size distribution histograms of Pt NCs. 200 particles were counted to calculate the average size. The concentrations of aniline monomer and  $\text{K}_2\text{PtCl}_4$  are 2.81 mM and 1.56 mM in 4 mL solution, respectively.

*Synthesis of 3D network PANI/Pt NCs.* When the as-obtained 3D network PANI was added into the mixture solution (containing Pt precursor, HCOOH, and water for a certain time), 3D network PANI/Pt NCs were received. Unless specified, 3D network CTAC-PANI was used as the supporting material here. As shown in Fig. 3a, high-density NCs spontaneously loaded on the surface of 3D network PANI. The NCs have monodispersed diameters (approximately 2-3 nm, 200 particles were counted to calculate the average size). Fig. 3b shown the HRTEM lattice image of the NCs. The lattice spacing of NCs is 0.226 nm, which is consistent with that of Pt (111) planes. The obtained polyaniline nanofibers have a rougher surface compared to original PANI nanofibers surface (Fig. 1), indicating that Pt NCs were successfully deposited on the surface of PANI.

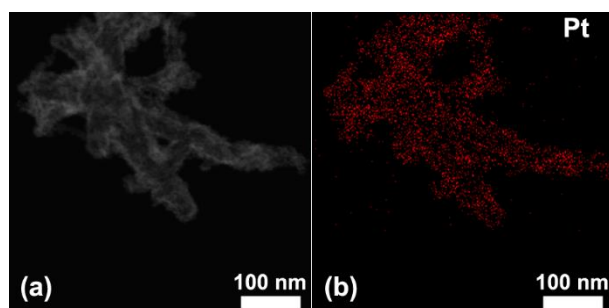


**Figure 4.** HAADF-STEM image (a) and HAADF-STEM-EDS mapping image (b) of 3D network PANI/Pt NCs.

Besides, the Pt element (red colour) distribution was shown in the EDS mapping profile of Fig. 4. From the HAADF-STEM image, the surface of 3D network PANI is loaded with ultra-high density Pt NCs. The EDS spectrum of 3D network PANI/Pt NCs shows that the Pt peak has a high intensity (Fig. S3). The EDS spectrum with highest intensity (not marked) is caused by the copper grids. Results indicated that the 3D network PANI played an important role for the homogeneous high-density loading and dispersion of the Pt NCs. The small size, monodispersed diameters, and homogeneous loading of the Pt NCs on the surface of 3D network PANI are important for enhancing the electrocatalysis performance.

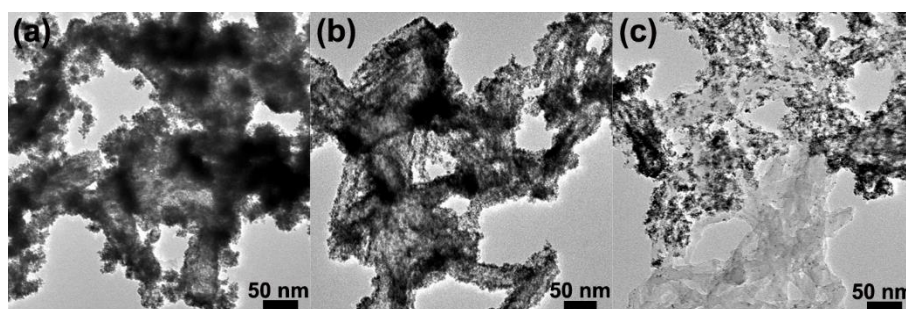


**Figure 5.** TEM images of 3D network PANI/Pt NCs at different amount of aniline monomer: (a) 0.56 mM, (b) 2.81 mM, and (c) 3.75 mM. The concentration of  $K_2PtCl_4$  is 1.56 mM in 4 mL solution.

Fig. 5 shows the TEM images of 3D network PANI/Pt NCs with different initial concentration of PANI. High density and monodisperse Pt NCs were well-dispersed on the surface of the 3D network PANI (Fig. 5b) at optimal conditions. Too little PANI matrix leads to severe aggregation of Pt nanocrystals which can be seen in Fig. 5a. When increasing the amount of 3D network PANI, Pt NCs could not cover the surface of 3D network PANI. Besides, 3D network DTAC-PANI was also used as supporting materials, the results are similar to that of 3D network CTAC-PANI (Fig. S4). When decreasing or increasing the amount of 3D network DTAC-PANI, Pt NCs could not well disperse on the surface of the 3D network DTAC-PANI (Fig. S4a and S4c). Only under specific condition, high density Pt NCs could adsorb on the surface of 3D network DTAC-PANI well (Fig. S4b). Thus, the result indicates high-density Pt NCs could well disperse on the surface of 3D network PANI (3D network CTAC-PANI or DTAC-PANI).

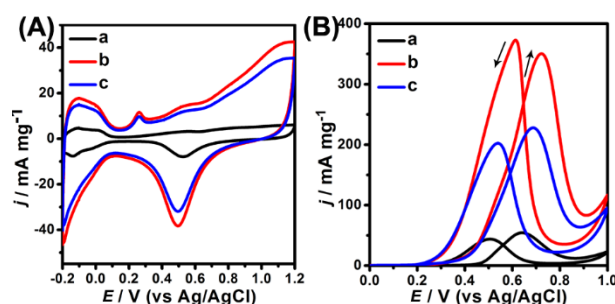


**Figure 6.** CV curves (A and B) of GCEs modified by 3D network PANI/Pt NCs at different amount of aniline monomer measured in 0.50 M  $\text{H}_2\text{SO}_4$  solution in the absence (A) and presence (B) of 1.0 M methanol: (a, black curve) 0.56 mM, (b, red curve) 2.81 mM, and (c, blue curve) 3.75 mM. The currents are normalized by the Pt mass loaded on the GCE. The scan rates are  $50 \text{ mV s}^{-1}$  (A) and  $20 \text{ mV s}^{-1}$  (B).

Here, in order to select the best catalyst (Table S1), we examined and compared all the 3D network PANI/Pt NCs products by measuring their catalytic activity in methanol oxidation. The electrochemically active surface area (ECSA) of 3D network PANI/Pt NCs with 2.81 mM of aniline monomer has the highest value,  $29.1 \text{ m}^2 \text{ g}^{-1}$  (Fig. 6A). Similarly, such 3D network PANI/Pt NCs modified GCE exhibits best electrocatalytic performance according to the highest mass normalized current density (Fig. 6B). The peak of mass-normalized current density of 3D network PANI/Pt NCs under optimal condition is  $350.4 \text{ mA mg}^{-1}$  in the positive-going scan. When the supporting material was changed to 3D network DTAC-PANI, the electrocatalysis results are similar to that of 3D network CTAC-PANI/Pt NCs (Fig. S5). The 3D network DTAC-PANI/Pt NCs with 2.81 mM of aniline monomer has the highest ECSA value ( $26.7 \text{ m}^2 \text{ g}^{-1}$ ) and electrocatalytic activity ( $306.3 \text{ mA mg}^{-1}$ ). When the amount of 3D network PANI was significantly reduced, the aggregation of Pt NCs on the surface of 3D network PANI leads to the decrease of their electrocatalytic activity (Fig. 6B and Fig. S5B, a, black curve). When the amount of 3D network PANI is excessive, the current density of the 3D network PANI/Pt NCs catalyst is still lower (Fig. 6B and Fig. S5B, c, blue curve). It can be summarized from electrocatalytic results that the 3D network CTAC-PANI/Pt NCs always have higher ECSA value and better electrocatalytic activity. The entire electrocatalysis data are listed in Table S1. The electrocatalysis results are

the same as that of Cr(VI) adsorption. Amino and benzene groups in 3D network PANI can stabilize Pt NCs. 2-3 nm Pt NCs will be located on surfaces of PANI by interactions between Pt NCs with polymer matrix with ultra-high density. The larger surface area and strong interactions between Pt NCs and the 3D network PANI support lead to high electrocatalytic performance.

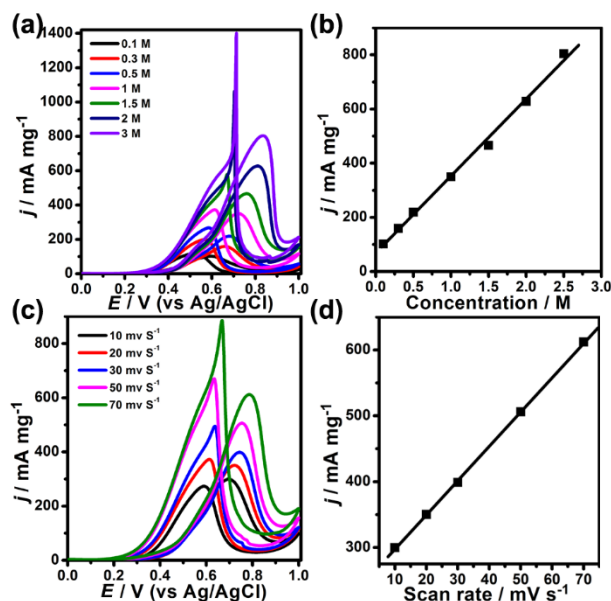


**Figure 7.** (a) Cyclic voltammograms (CVs) curves of 3D network CTAC-PANI/Pt NCs modified GCEs at different methanol concentrations bearing 0.5 M H<sub>2</sub>SO<sub>4</sub>. (b) Plot of calibrated oxidation peak current vs. methanol concentration. The scan rate is 20 mV s<sup>-1</sup>. (c) CV curves of 3D network PANI/Pt NCs modified GCEs at 1.0 M methanol bearing 0.5 M H<sub>2</sub>SO<sub>4</sub> at different scan rates. Scan rates were 10, 20, 30, 50, and 70 mV s<sup>-1</sup>, respectively. (d) Plot of calibrated oxidation peak current vs. scan rate. The concentrations of aniline monomer and K<sub>2</sub>PtCl<sub>4</sub> are 2.81 mM and 1.56 mM in synthesis of 3D network PANI/Pt NCs process, respectively.

Fig. 7a shows the CVs curves of 3D CTAC-PANI/Pt NCs modified GCEs for methanol oxidation at different methanol concentrations in 0.5 M H<sub>2</sub>SO<sub>4</sub> solution. Fig. 7b shows the calculated current density of 3D network PANI/Pt NCs modified GCEs, the linearly increases from 102.1 mA mg<sup>-1</sup> to 804.4 mA mg<sup>-1</sup> with increasing methanol concentration from 0.10 M to 3.0 M. The higher the methanol concentration, the more positive the oxidation peak position is. When the methanol concentration is higher than 3.0 M, the current intensity did not significantly continue to increase. Since The mass of catalyst on the GCE is certain, high concentration of medium gives rise to the higher activation barrier toward methanol oxidation. When the methanol concentration massive increased, the ability of the oxidation of freshly chemisorbed species from methanol adsorption decreased. This may cause the positive shift of oxidation peak position with increasing the methanol concentration. Fig. 7c demonstrates the effect of scan rates on the electrochemical oxidation of methanol in the acid solution. The slower the scan rate, the lower the oxidation current is in the negative potential scan. Fig. 7d shows a fairly linear relationship between the current density of oxidation peak and the scan rate, indicating that the electrode reaction is a surface-controlled process [37].

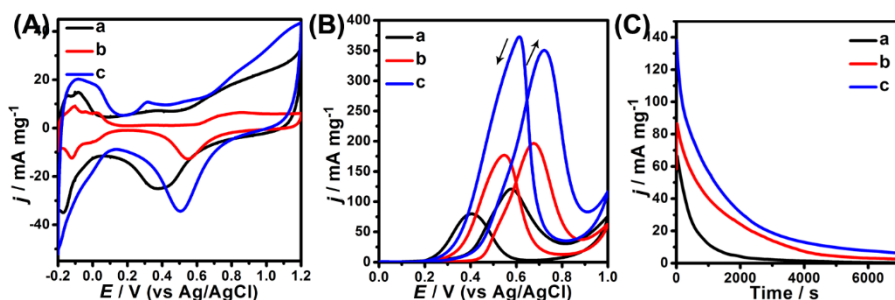


**Figure 8.** CV curves (A and B) and CA curves (C) of the GCE modified by commercial Pt black (a, black curve), hyperbranched Pt NCs (b, red curve), and 3D network PANI/Pt NCs (c, blue curve) measured in 0.50 M H<sub>2</sub>SO<sub>4</sub> solution in the absence (A) and presence (B and C) of 1.0 M methanol. The scan rates of (A) and (B and C) are 50 mV s<sup>-1</sup> and 20 mV s<sup>-1</sup>, respectively. CA curves (C) are recorded at 0.50 V. The currents are normalized by the Pt mass loaded.

Based on the above results, the 3D network CTAC-PANI/Pt NCs with 2.81 mM of aniline monomer is the best candidate for methanol oxidation catalysis. In order to investigate its potential use as anodes in DMFCs, the electrocatalytic behavior of prepared 3D network PANI/Pt NCs, commercial Pt black and spherical hyperbranched Pt NCs on methanol oxidation was studied (Fig. S6). The ECSA values of these three candidates are calculated and shown in Fig. 8A. The ECSA value of the 3D network PANI/Pt NCs modified GCE (29.1 m<sup>2</sup> g<sup>-1</sup>) is about 1.94-fold higher than that of hyperbranched Pt NCs (15.0 m<sup>2</sup> g<sup>-1</sup>) and 2.06-fold higher than that of commercial Pt black electrodes (14.1 m<sup>2</sup> g<sup>-1</sup>). Fig. 8B shows the CV curves of the commercial Pt black modified, spherical hyperbranched Pt NCs modified and PANI/Pt NCs modified GCE electrode, respectively. The mass-normalized current density of 3D network PANI/Pt NCs is 350.4 mA mg<sup>-1</sup>, which is about 1.75 times and 2.92 times higher than that of spherical hyperbranched Pt NCs (200 mA mg<sup>-1</sup>) and the commercial Pt black (120 mA mg<sup>-1</sup>), respectively. The results shown that the 3D network PANI/Pt NCs composites owned best catalytic performance compared to the commercial Pt black and hyperbranched Pt NCs. To further investigate the durability of prepared catalyst, the long-term methanol oxidation process were performed using commercial Pt black, spherical hyperbranched Pt NCs, and 3D network PANI/Pt NCs as catalyst. According to their chronoamperometric (CA) curves, the 3D network PANI/Pt NCs shown better electrochemical stability than the spherical hyperbranched Pt NCs or commercial Pt black (Fig. 8C). Fig. S7 shows that the oxidation peak current density of 3D network PANI/Pt NCs is reduced by less than 40% after 500 cycles of methanol oxidation process.

To further understand the effect of structure and morphology of PANI on methanol oxidation, a series of electrocatalysis comparison tests using other shape of PANI as supporting materials was performed. Fig. S8 shows TEM images of 1D PANI nanofiber and PANI hydrogel in the absence and presence of high density distribution of small Pt NCs. CV curves of the GCE modified by all different catalyst were shown in Fig. S9. The ECSA value of 1D PANI nanofiber/Pt NCs and PANI hydrogel/Pt NCs is 27.2 and 19.4 m<sup>2</sup> g<sup>-1</sup>, respectively (Table 1). The ECSA value is 1.92-fold and 1.38-fold higher than that of commercial Pt black electrodes (14.1 m<sup>2</sup> g<sup>-1</sup>), but it is lower than that of 3D network PANI/Pt NCs (29.1 m<sup>2</sup> g<sup>-1</sup>). The mass-normalized current density of 1D PANI nanofiber/Pt NCs (203.9 mA mg<sup>-1</sup>) and PANI hydrogel/Pt NCs (249.6 mA mg<sup>-1</sup>) are also higher than that of commercial Pt black

electrodes ( $120 \text{ mA mg}^{-1}$ ) and lower than that of 3D network PANI/Pt NCs ( $350.4 \text{ mA mg}^{-1}$ ) in the positive-going scan (Fig. S10 and Table 1). In general, in comparison with commercial Pt black, spherical hyperbranched Pt NCs and other structure PANI/Pt NCs, highest electrocatalytic activity of 3D network PANI/Pt NCs result from three major factors: 1) the high conductivity of PANI in acidic conditions result in faster electron transfer between methanol and Pt NCs; 2) the 3D network structure of PANI have larger surface area; 3) the high density distribution of small and uniform Pt NCs (2-3 nm) on the surface of 3D network PANI increased the effective electrocatalysis active area.

**Table 1.** Comparison of electrocatalytic activity of Pt-based catalyst in methanol oxidation.

Samples	Method for preparation	ECSA ( $\text{m}^2 \text{g}^{-1}$ )	Reference
PtRuCu nanocrystalline	Solvothermal method	52.28	[38]
Pt/zeolite	Chemical impregnation	15.95	[39]
Pt/RGO/PANI	In-situ reduction	42.16	[40]
Pt-Co	Self-assembly	29.79	[41]
Pt-Ru nanocrystal	Soft template	72.1	[42]
Pt/polyaniline	In-situ reduction	29.1	This work

In addition, in order to assess the performance of prepared catalyst, a comparison on ECSA is given in Table 1. Results show the comprehensive comparison based on Pt-based catalyst for methanol oxidation reaction. It can be easily found that the Pt-Ru nanocrystals owned the highest catalytic activity due to their excellent catalytic performance naturally. When matrix was used for fabricating catalyst compound-in order to enhance the price of prepared catalyst compound, electron conduction is essential for improve the ECSA since the zeolite used as matrix has lowest ECSA number.

#### 4. CONCLUSION

In summary, a simple strategy has been reported for synthesis of three dimensions (3D) network PANI towards fabricating Pt-based catalyst for methanol oxidation. 3D network PANI consists of interconnected uniform PANI nanofibers with diameters of approximately 40 nm and show excellent removal performance for Cr(VI) due to the three-dimensional porous structure and large surface area. The adsorption capacity of 3D network CTAC-PANI is up to  $263.5 \text{ mg g}^{-1}$ . Moreover, 3D network PANI/Pt NCs was received after deposition of Pt nanocrystals on the PANI skeleton. It is found that ultra-high density small Pt NCs with a diameter of about 2-3 nm could be facilely deposit on the surface of 3D network PANI. Furthermore, 3D network PANI/Pt NCs shows excellent methanol oxidation performance. In comparison with commercial Pt black ( $120 \text{ mA mg}^{-1}$ ) and other structure PANI/Pt NCs, the 3D network PANI/Pt NCs have superior catalytic activity ( $350.4 \text{ mA mg}^{-1}$ ) towards methanol oxidation due to the conductivity of PANI, large surface area of 3D network PANI, and high density distribution of small Pt NCs on the surface of 3D network PANI.

## NOTES

The authors declare no competing financial interest.

## ACKNOWLEDGEMENTS

This work is financially supported by the National Natural Science Foundation of China (21503121) and Foundation of Shandong province (ZR2017BB064, J17KA115). J. Duan thanks National Natural Science Foundation of China (21607096) and the Promotive Research Fund for Excellent Young and Middle-aged Scientists of Shandong Province (BS2015CL008).

## SUPPLEMENTARY MATERIAL

### Experimental section

#### 1. Synthesis of PANI nanofibers

The PANI nanofibers were synthesized according to a previously published protocol [1]. Typically, an aqueous solution of aniline (0.32 M) in 1 M doping hydrochloric acid (10 mL) and another solution of ammonium peroxydisulfate (0.08 M) in the same doping acid (10 mL) were prepared and mixed. When the color of solution changed to green, PANI nanofibers were synthesized. After washing with ethanol and water to remove the residual surfactant, PANI nanofibers were prepared.

#### 2. Synthesis of PANI hydrogel

The PANI hydrogel was synthesized following published literature [2]. The hydrogel was synthesized by mixing solution A and solution B. Solution A was prepared by dissolving 0.921 mL phytic acid in 2 mL of water while stirring. Next, 0.458 mL of the aniline monomer was added to the solution. Solution B was 1 mL ammonium persulfate solution (1.25 mM). When solution A and B were mixed, the color of the mixed solution changed to dark green. After 3 min, the PANI hydrogel was formed.

#### 3. Synthesis of PANI nanofibers/Pt NCs and PANI hydrogel/Pt NCs

PANI nanofibers (or PANI hydrogel) and 250  $\mu$ L of  $K_2PtCl_4$  solution (0.025 M) were added to 3.00 mL of water solution under stirring. Few minutes later, 750  $\mu$ L of formic acid was added into the mixture solution containing Pt precursor. Then, when the color of the reaction solutions gradually changed from green to dark, PANI nanofibers/Pt NCs (or PANI hydrogel/Pt NCs) were obtained.

## References

1. Huang JX and Kaner RB, *Angew. Chem. Int. Ed.*, 43 (2004) 5817.
2. Zhai DY, Liu B, Shi Y, Pan LJ, Wang YQ, Li WB, Zhang R and Yu GH, *ACS Nano*, 7 (2013) 3540.



Fig. S1 Digital photograph of 3D network PANI gel.

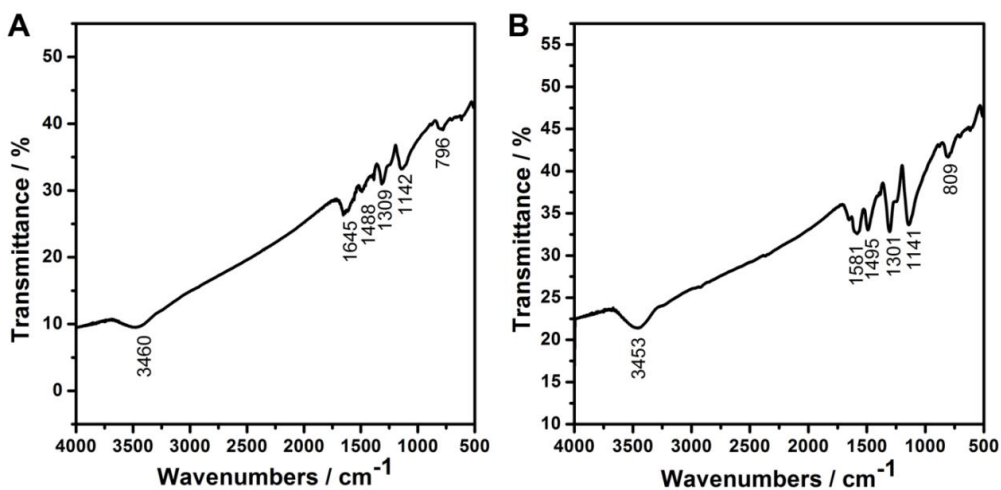


Fig. S2 FTIR spectra of 3D network CTAC-PANI gel (A) and DTAC-PANI gel (B).

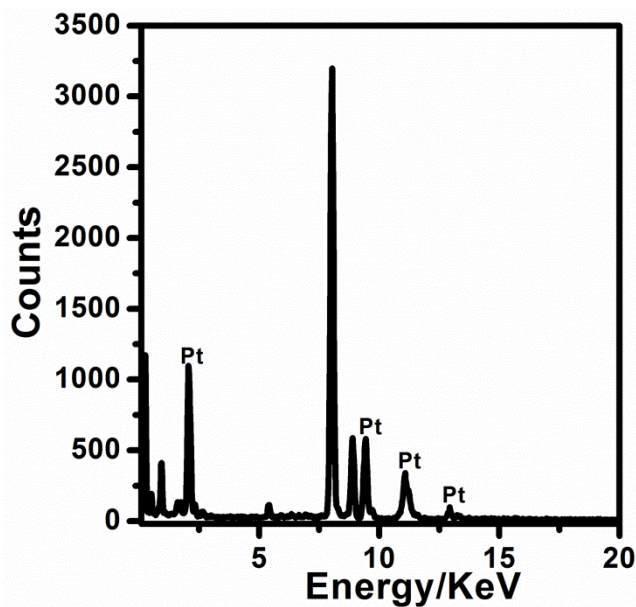
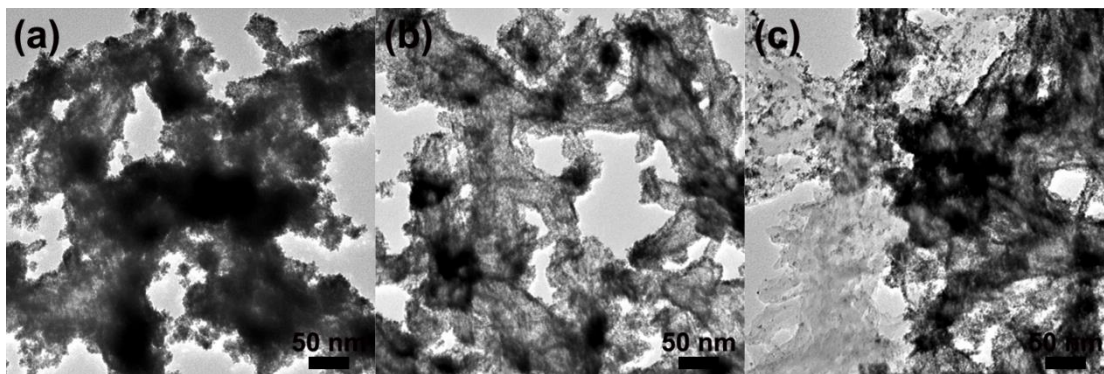
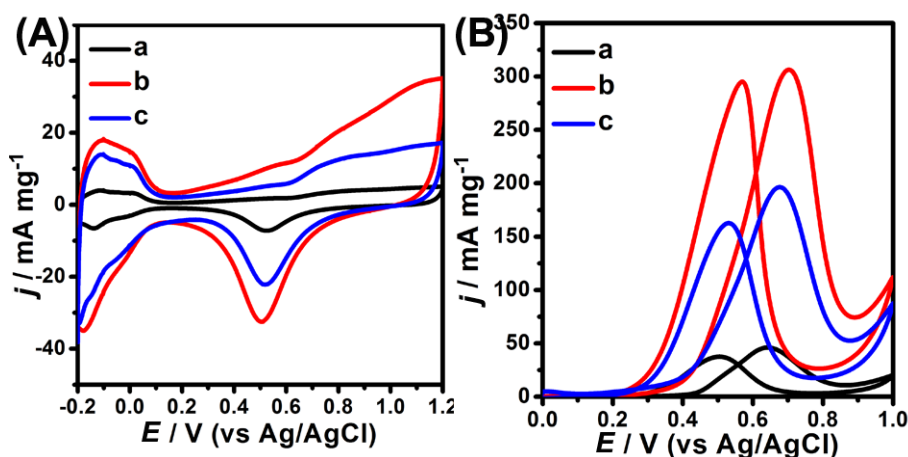


Fig. S3 EDS spectrum of 3D network PANI/Pt NCs.



**Fig. S4** TEM images of 3D network DTAC-PANI/Pt NCs at different amount of aniline monomer: (a) 0.56 mM, (b) 2.81 mM, and (c) 3.75 mM. The concentration of  $K_2PtCl_4$  is 1.56 mM in 4 mL solution.



**Fig. S5** CV curves (A and B) of GCEs modified by 3D network DTAC-PANI/Pt NCs at different amount of aniline monomer measured in 0.50 M  $H_2SO_4$  solution in the absence (A) and presence (B) of 1.0 M methanol: (a, black curve) 0.56 mM, (b, red curve) 2.81 mM, and (c, blue curve) 3.75 mM. The currents are normalized by the Pt mass loaded on the GCE. The scan rates are  $50 \text{ mV s}^{-1}$  (A) and  $20 \text{ mV s}^{-1}$  (B).

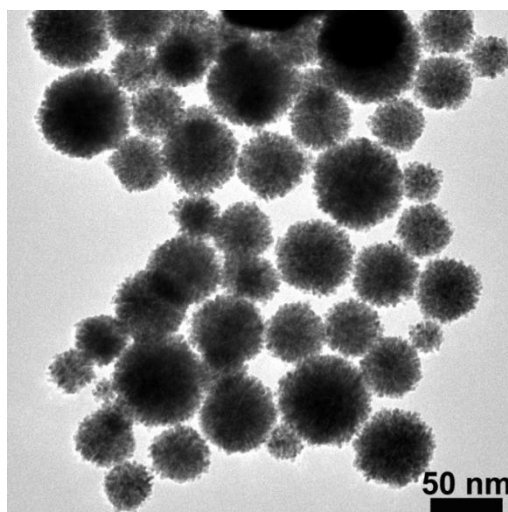


**Fig. S6** TEM image of hyperbranched Pt NCs.

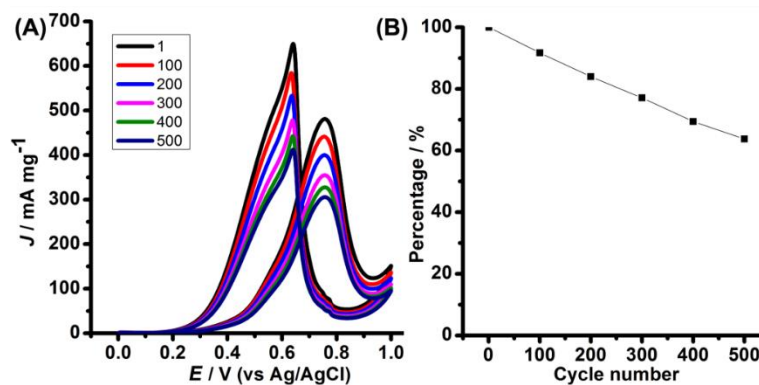


**Fig. S7** (A) CV curves of 3D network PANI/Pt NCs at different scanning cycle number. (B) Plot of the calibrated CV oxidation peak current density vs. the scanning cycle number.

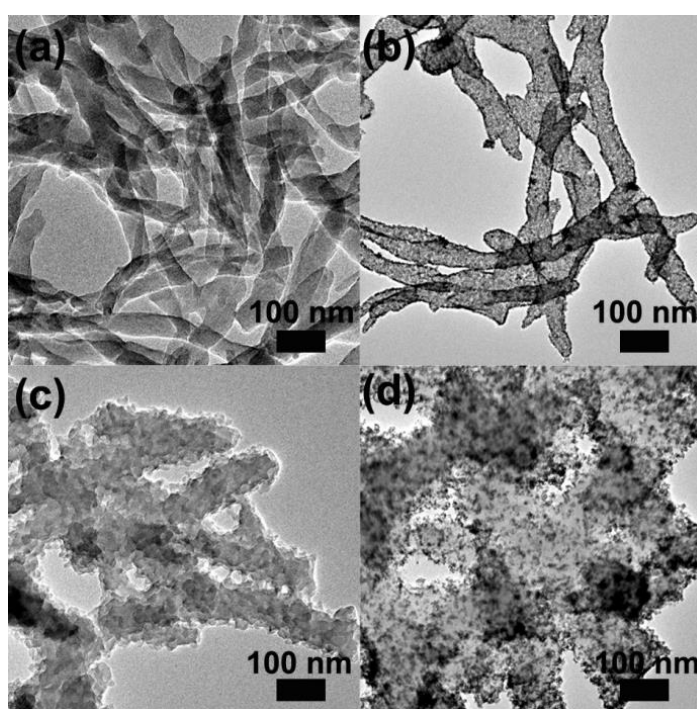


**Fig. S8** TEM images of PANI nanofiber (a and b) and PANI hydrogel (c and d) in the absence (a and c) and presence (b and d) of Pt NCs.

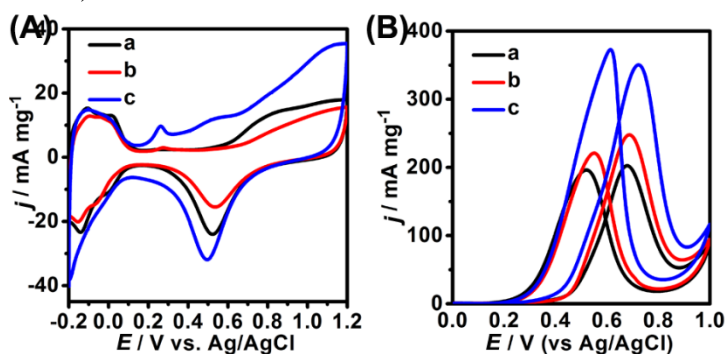


**Fig. S9** CV curves (A and B) of the GCE modified by PANI nanofiber/Pt NCs (a, black curve), PANI hydrogel/Pt NCs (b, red curve), and 3D network PANI/Pt NCs (c, blue curve) measured in 0.50 M  $\text{H}_2\text{SO}_4$  solution in the absence (A) and presence (B) of 1.0 M methanol. The scan rates of (A) and (B) are  $50 \text{ mV s}^{-1}$  and  $20 \text{ mV s}^{-1}$ , respectively. The currents are normalized by the Pt mass loaded.

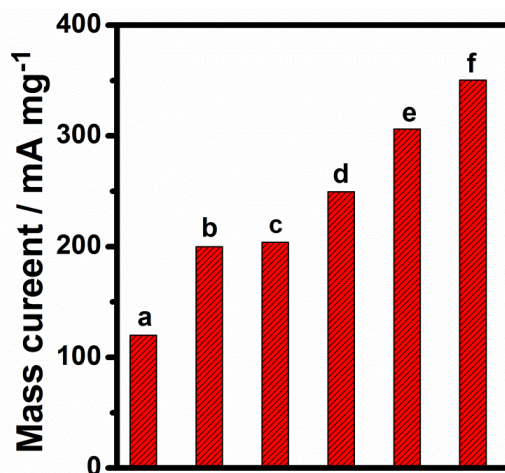


**Fig. S10** Mass activities for methanol oxidation in 0.5 M H<sub>2</sub>SO<sub>4</sub> solution on (a) commercial Pt black, (b) hyperbranched Pt NCs, (c) 1D PANI nanofiber/Pt NCs, (d) PANI hydrogel/Pt NCs, (e) 3D network DTAC-PANI/Pt NCs, (f) 3D network CTAC-PANI/Pt NCs. The scan rate is 20 mV s<sup>-1</sup>.

**Table S1** Summary of the experimental parameters, ECSA, and mass activities of 3D network PANI/Pt NCs

Samples	Sample image	Aniline / mM	ECSA / m <sup>2</sup> g <sup>-1</sup>	Mass activity / mA mg <sup>-1</sup>
CTAC-PANI/Pt NCs	Figure 5a	0.56	8.2	54.4
	Figure 5b	2.81	29.1	350.4
	Figure 5c	3.75	20.9	227.8
DTAC-PANI/Pt NCs	Figure S4a	0.56	6.8	46.1
	Figure S4b	2.81	26.7	306.3
	Figure S4c	3.75	18.2	196.4

## References

1. Wenhao Gong, Zheng Jiang, Rifeng Wu, Yang Liu, Lei Huang, Ning Hu and Panagiotis Tsiakaras, Pei Kang Shen, *Appl. Catal. B-Environ.*, 246 (2019) 277.
2. C.Z. Zhu, S.F. Fu, Q.R. Shi, D. Du and Y.H. Lin, *Angew. Chem. Int. Ed.*, 56 (2017) 13944.
3. T. Sheng, Y.F. Xu, Y.X. Jiang, L. Huang, N. Tian, Z.Y. Zhou, I. Broadwell and S.G. Sun, *Acc. Chem. Res.*, 49 (2016) 2569.
4. H.A. Miller, A. Lavacchi, F. Vizza, M. Marelli, F. D. Benedetto, F. D'Acapito, Y. Paska, M. Page and D.R. Dekel, *Angew. Chem. Int. Ed.*, 55 (2016) 6004.
5. W. Wang, F. Lv, B. Lei, S. Wan, M.C. Luo and S.J. Guo, *Adv. Mater.*, 28 (2016) 10117.
6. N. Ishiguro, S. Kityakarn, O. Sekizawa, T. Uruga, H. Matsui, M. Taguchi, K. Nagasawa, T. Yokoyama and M. Tada, *J. Phys. Chem. C*, 120 (2016) 19642.
7. A. Kongkanand, N.P. Subramanian, Y.C. Yu, Z.Y. Liu, H. Igarashi and D.A. Muller, *ACS Catal.*, 6 (2016) 1578.
8. O. Sorsa, H. Romar, U. Lassi and T. Kallio, *Electrochim. Acta*, 230 (2017) 49.
9. X. Q. Huang, Z.P. Zhao, L. Cao, Y. Chen, E.B. Zhu, Z.Y. Lin, M. Li, A.M. Yan, A. Zettl, Y.M.

- Wang, X.F. Duan, T. Mueller and Y. Huang, *Science*, 348 (2015) 1230.
10. V.C. Anitha, Raul Zazpe, Milos Krbal, JeongEun Yoo, Hanna Sopha, Jan Prikryl, Gihoon Cha, Stanislav Slang, Patrik Schmuki and Jan M. Macak, *J. Catal.*, 365 (2018) 86.
  11. L. Wang and Y. Yamauchi, *Chem. Mater.*, 21 (2009) 3562.
  12. X. Wang, L. Figueroa-Cosme, X. Yang, M. Luo, J.Y. Liu, Z.X. Xie and Y.N. Xia, *Nano Lett.*, 16 (2016) 1467.
  13. C. Chen, Y.J. Kang, Z.Y. Huo, Z.W. Zhu, W.Y. Huang, H.L. Xin, J.D. Snyder, D.G. Li, J.A. Herron, M. Mavrikakis, M.F. Chi, K.L. More, Y.D. Li, N.M. Markovic, G.A. Somorjai, P.D. Yang and V.R. Stamenkovic, *Science*, 343 (2014) 1339.
  14. P. Strasser, S. Koh, T. Anniyev, J. Greeley, K. More, C.F. Yu, Z.C. Liu, S. Kaya, D. Nordlund, H. Ogasawara, M.F. Toney and A. Nilsson, *Nat. Chem.*, 2 (2010) 454.
  15. N. Zhang, L.Z. Bu, S.J. Guo, J. Guo and X.Q. Huang, *Nano Lett.*, 16 (2016) 5037.
  16. S. Mourdikoudis, M. Chirea, T. Altantzis, I. Pastoriza-Santos, J. Pérez-Juste, F. Silva, S. Bals and L.M. Liz-Marzán, *Nanoscale*, 5 (2013) 4776.
  17. Y.J. Li, W.C. Ding, M.R. Li, H.B. Xia, D.Y. Wang and X.T. Tao, *J. Mater. Chem. A*, 3(2015) 368.
  18. Q.R. Shi, Y. Song, C.Z. Zhu, H.P. Yang, D.Du and Y.H. Lin, *ACS Appl. Mater. Interfaces*, 7 (2015) 24288.
  19. C. Gumeci, A. Marathe, R.L. Behrens, J. Chaudhuri and C. Korzeniewski, *J. Phys. Chem. C*, 11 (2014) 14433.
  20. Y.J. Kang, J.B. Pyo, X.C. Ye, R.E. Diaz, T.R. Gordon, E.A. Stach and C.B. Murray, *ACS Nano*, 7 (2013) 645.
  21. S.C. Lin, C.S. Hsu, S.Y. Chiu, T.Y. Liao and H.M. Chen, *J. Am. Chem. Soc.*, 139 (2017) 2224.
  22. B.Y. Xia, H.B. Wu, N. Li, Y. Yan, X.W. Lou and X. Wang, *Angew. Chem. Int. Ed.*, 54 (2015) 3797.
  23. J. Zhao, L.Q. Zhang, T. Chen, H. Yu, L. Zhan, H. Xue and H.Q. Hu, *J. Phys. Chem. C*, 116 (2012) 21374.
  24. I.D. Choi, H. Lee, Y.B. Shim and D. Lee, *Langmuir*, 26 (2010) 11212.
  25. H. Xu, A.L. Wang, Y.X. Tong and G.R. Li, *ACS Catal.*, 6 (2016) 5198.
  26. A.J. Xie, F.Tao, L.N. Hu, Y.F. Li, W.L. Sun, C. Jiang, F.F. Cheng, S.P. Luo and C. Yao, *Electrochim. Acta*, 231 (2017) 502.
  27. S.G. Chen, Z.D. Wei, X.Q. Qi, L.C. Dong, Y.G. Guo, L.J. Wan, Z.G. Shao and L. Li, *J. Am. Chem. Soc.*, 134 (2012) 13252.
  28. S.J. Guo, S.J. Dong and E.K. Wang, *small* 5 (2009) 1869.
  29. R.W. Yan and B.K. Jin, *Electrochim. Acta*, 115 (2014) 449.
  30. G.C. Li and Z.K. Zhang, *Macromolecules*, 37 (2004) 2683.
  31. L.J. Pan, G.H. Yu, D.Y. Zhai, H.R. Lee, W.T. Zhao, N. Liu, H.L. Wang, B.C.K. Tee, Y. Shi, Y. Cui and Z.N. Bao, *Proc Natl Acad Sci.*, 109 (2012) 9287.
  32. D.Y. Zhai, B. Liu, Y. Shi, L.J. Pan, Y.Q. Wang, W.B. Li, R. Zhang and G.H. Yu, *ACS Nano*, 7 (2013) 3540.
  33. L.L. Li, Y.Q. Wang, L.J. Pan, Y. Shi, W. Cheng, Y. Shi and G.H. Yu, *Nano Lett.*, 15 (2015) 1146.
  34. B. Qiu, C.X. Xu, D.Z. Sun, Q. Wang, H.B. Gu, X. Zhang, B.L. Weeks, J. Hopper, T.C. Ho, Z.H. Guo and S.Y. Wei, *Appl. Surf. Sci.*, 334 (2015) 7.
  35. H.Y. Yu, C.S. Wang, J.H. Zhang, H.S. Li, S.X. Liu, Y. Ran and H.B. Xia, *Mater. Chem. Phys.*, 133 (2012) 459.
  36. L. Tang, Y. Fang, Y. Pang, G.M. Zeng, J.J. Wang, Y.Y. Zhou, Y.C. Deng, G.D. Yang, Y. Cai and J. Chen, *Chem. Eng. J.*, 254 (2014) 302.
  37. H.B. Xia, Y. Ran, H.S. Li, X.T. Tao and D.Y. Wang, *J. Mater. Chem. A*, 1 (2013) 4678.  
Shengfeng Xue, Wentao Deng, Fang Yang, Jinlong Yang, Ibrahim Saana Amiin, Daping He, Haolin Tang, and Shichun Mu, *ACS catal.*, 8 (2018) 7578.
  38. A. Medina Ramirez, B. Ruiz Camacho, M. Villcaña Aguilera, I.R. Galindo Esquivel and J.J. Ramírez-Minguela, *Appl. Surf. Sci.*, 456 (2018) 204.

39. Sinan Eris, Zeynep Das, delen, Yunus Yldz and Fatih Sen, *Int. J. Hydrogen. Energy*, 43 (2018) 1337.
40. Lu Zhang, Xiao-Fang Zhang, Xue-Lu Chen, Ai-Jun Wang, De-Man Han, Zhi-Gang Wang and
41. Jiu-Ju Feng, *J. Colloid Interf. Sci.*, 536 (2019) 556.
42. Liang Huang, Xueping Zhang, Qingqing Wang, Yujie Han, Youxing Fang and Shaojun Dong, *J. Am. Chem. Soc.*, 140 (2018) 1142.

© 2020 The Authors. Published by ESG ([www.electrochemsci.org](http://www.electrochemsci.org)). This article is an open access article distributed under the terms and conditions of the Creative Commons Attribution license (<http://creativecommons.org/licenses/by/4.0/>).